

Electron Spin Resonance of the Excited ${}^2E(3d^3)$ Level of Cr^{3+} and V^{2+} in MgO †

LLOYD L. CHASE*

Laboratory of Atomic and Solid State Physics, Cornell University, Ithaca, New York

(Received 14 November 1967)

The electron spin resonance of the 2E level of the isoelectronic $3d^3$ ions, V^{2+} and Cr^{3+} , in MgO is examined using an optical-detection technique. Sizeable, anisotropic g shifts are observed, which are quantitatively accounted for by the orbital moment admixed into 2E by configuration mixing and spin-orbit coupling. The hfs observed for V^{51} is in agreement with quantitative estimates based on the observed g shift. The resonances observed optically are anisotropically broadened and show sample-dependent asymmetries. The broadening is found to result from the influence of random local strain on the orbital degeneracy of 2E . Asymmetric resonances are expected on the basis of the selection rules for the circular-polarized fluorescence used to detect the resonances. These effects are modified considerably by the details of thermal and cross relaxation among the four sublevels of 2E . On this basis, the sample dependence of the resonance shapes is attributed to a type of cross relaxation due to the presence of Fe^{2+} in varying quantities in the samples studied. Samples having spin-lattice relaxation rates for 2E which agree with those calculated from static-strain-splitting data have asymmetric resonances of the type expected from the fluorescence selection rules.

I. INTRODUCTION

BECAUSE of its unique optical properties and its importance in laser applications, the trivalent chromium ion in octahedral coordination has been used as a model for many of the refinements to crystal-field calculations and the study of phenomena associated with electronic excitation in crystals. The most common host material for these studies has been the trigonal aluminum-oxide lattice in which the lack of inversion symmetry leads to the sharp, intense, electric dipole R -line emission. The initial state for this fluorescence is the 2E level of the $3d^3$ configuration, which has been the object of numerous optical investigations and has also been studied by ESR using optical-detection techniques.

Many studies have also been made on the chromium ion in MgO . Because of the cubic symmetry of the predominant chromium substitutional site in this host, the R -line fluorescence is a weak magnetic dipole transition.¹ However, as a model system, $\text{MgO}:\text{Cr}^{3+}$ is complementary in many ways to ruby because of the absence of the trigonal field, which often obscures the effects of other interactions on the electronic levels. In particular, the 2E level is orbitally degenerate in MgO , and its properties when split by applied uniaxial strain and magnetic field have been studied optically.

The measured strain-splitting coefficients^{2,3} show a relatively weak lattice coupling, and the Zeeman effect results for the isoelectronic V^{2+} ion⁴ display a magnetic-

field-dependent broadening of the Zeeman components which is suggestive of a magnetic splitting of the orbital degeneracy. For a more detailed study of these properties, it is desirable to utilize the improved resolution of ESR. This paper reports the results of such a study, employing an optical-detection technique as was used for the case of ruby by Geschwind *et al.*⁵⁻⁷

II. EXPERIMENTAL

The methods employed in optical detection of ESR in excited states have been discussed previously.⁵ Briefly summarized, the population changes induced by ESR transitions in the excited state may be detected by either monitoring a particular Zeeman component in the fluorescence from the state or by isolating either circular-polarization component of the fluorescence along the applied magnetic field.

Figure 1 shows the longitudinal Zeeman selection rules for the magnetic dipole R -line transition in MgO for \mathbf{H} along a cube axis.¹ It is apparent from this that equal and opposite changes result in the intensities of the two circular polarizations when the populations of the 2E spin levels are altered. The same is true of the intensities of the two Zeeman components, although the relative change is twice as large as for the circular polarizations. However, only a very small fraction of the fluorescence is passed through the slit of a spectrograph with the resolution necessary to separate these components, whereas $f/4$ optics were possible in monitoring circular polarizations. Because the shot noise due to photon statistics limited the signal-to-noise in this work, circular-polarization detection was used.

A simplified diagram of the experimental arrangement is shown in Fig. 2. The samples are ground into cylinders with axes oriented along a $\langle 110 \rangle$ crystalline

† Research supported in part by the U.S. Atomic Energy Commission under Contract No. AT(30-1)-2150, Technical Report No. NYO-2150-39, and by the Advanced Research Projects Agency through the Materials Science Center at Cornell University, Report No. 825.

* Present address: Bell Telephone Laboratories, Murray Hill, N. J.

¹ S. Sugano, A. L. Schawlow, and F. Varsanyi, *Phys. Rev.* **122**, 2045 (1960).

² A. L. Schawlow, A. H. Pinks, and S. Sugano, *Phys. Rev.* **122**, 1469 (1961).

³ M. D. Sturge, *Phys. Rev.* **131**, 1456 (1963).

⁴ M. D. Sturge, *Phys. Rev.* **130**, 639 (1963).

⁵ S. Geschwind, G. E. Devlin, R. L. Cohen, and S. R. Chinn, *Phys. Rev.* **137**, A1087 (1965).

⁶ S. Chinn, G. Devlin, F. Imbusch, and S. Geschwind, *Bull. Am. Phys. Soc.* **10**, 56 (1965).

⁷ G. F. Imbusch and S. Geschwind, *Phys. Letters* **18**, 109 (1965).

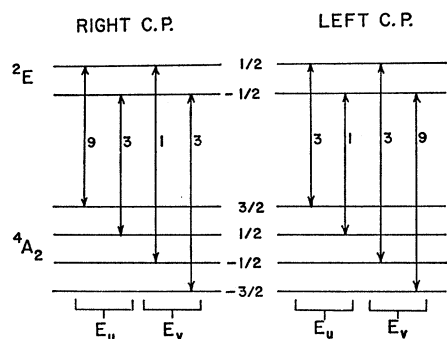


FIG. 1. Circular-polarization intensities for fluorescence along an applied magnetic field along [001].

axis so that data may be obtained for \mathbf{H} along all major cube axes. This cylinder is mounted along the axis of a full-wave cylindrical cavity which is terminated at the bottom end with a microwave short. A base of the cylindrical sample is mounted over an optical-pumping hole in the short, and both short and sample are rotated about their axes by means of a gear and pinion arrangement shown in Fig. 3.

The fluorescence is detected along the field through a hole in the cavity side wall and is passed through a circular polarizer, a light pipe running through a hole in the magnet pole piece, a narrow-band interference filter centered on the R -line fluorescence, and is detected by a cooled RCA 7102 photomultiplier.

The microwaves incident on the cavity are square-wave-modulated, allowing synchronous detection of the light signal. The output of the Osram HBO-200 Mercury arc used for the optical pumping has a large flicker component. This noise could be reduced below the fluorescent shot-noise level because the spin-lattice relaxation time in 2E is much shorter than the fluorescence decay time. This allows working at high microwave chopping rates, so that the corresponding flicker

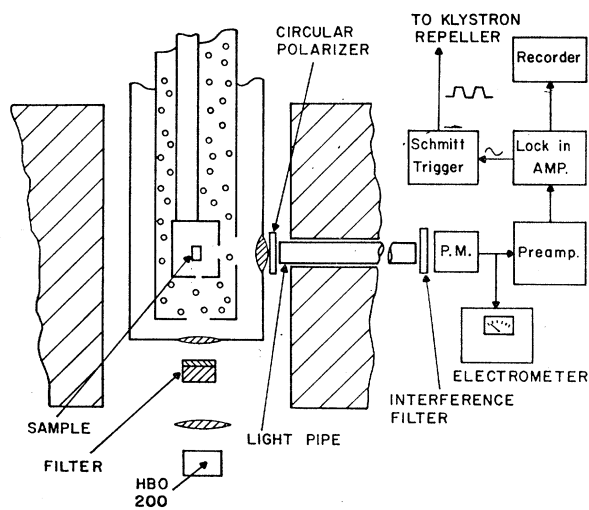


FIG. 2. Schematic of apparatus for optical detection of ESR.

components are filtered out by the fluorescent decay time, which is about 10 msec.

The samples were obtained from the Norton Company of Canada and had concentrations ranging from 0.02 to 0.2% of Cr^{3+} and 0.09% of V^{2+} , as measured from ESR calibrations, using the ground-state resonances. The vanadium samples were reduced from the normal trivalent state by the usual procedure of heating them in H_2 atmosphere at 1800°C for 10 h.⁴ A typical sample size was 3 mm in diam and 6 mm long.

Relaxation-time measurements, which aided in interpreting the resonance shapes, were carried out in most cases by averaging the circular-polarization decay dur-

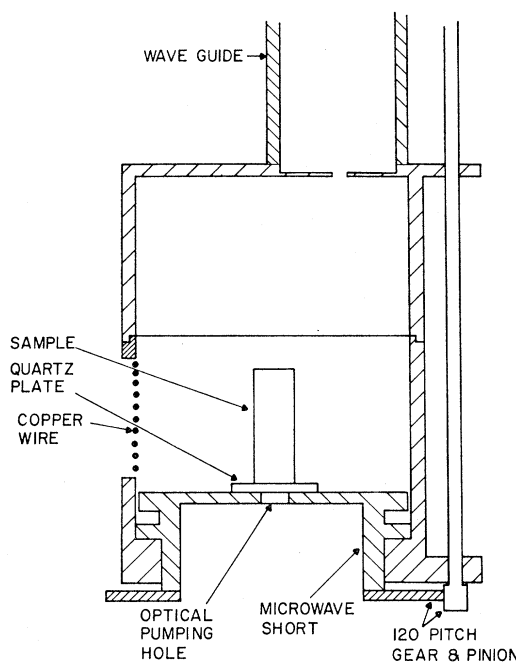


FIG. 3. Cross section of cylindrical microwave cavity with optical-pumping and detection holes.

ing the "off" portion of the microwave cycle, using a Nuclear Data Corporation "Enhancertron."

III. OBSERVED ESR SPECTRA

The ESR signals observed for the 2E level of Cr^{3+} , using optical detection, had sample-dependent shapes for which an explanation is given later. Representative data taken on samples with almost identical Cr^{3+} concentrations of 0.02% are shown in Figs. 4 and 5 and will be designated spectra I and II, respectively. These traces are taken at 1.5°K and a frequency of 23.0 GHz.

The peak signal observed in Fig. 4(a) corresponds to a total change in monitored light intensity of about 1%. It is estimated that the population of the 2E level in this case was about 10^{14} .

In I, for $\mathbf{H} \parallel [111]$, the resonance is a narrow line with 10- to 12-G width [the line shown in Fig. 4(a)]

is slightly broadened by the width of the saturated hole] and is located at $g=1.905\pm 0.001$. This line broadens and becomes symmetrically double-peaked as \mathbf{H} is rotated away from $[111]$ in a $\{110\}$ plane. The separation of the peaks has maxima along $[110]$ and $[001]$ directions of 400 and 800 G, respectively, at 23 GHz. The low-field peak of the $[001]$ resonance is very near to $g=2.000$, and the centroid of the doublet peaks remains at $g=1.905$ within the accuracy of the measurement. The "hole" in the resonance at $g=1.98$ is caused by changes in the reabsorption of the circularly polarized line fluorescence as the ground-state spin levels are saturated.

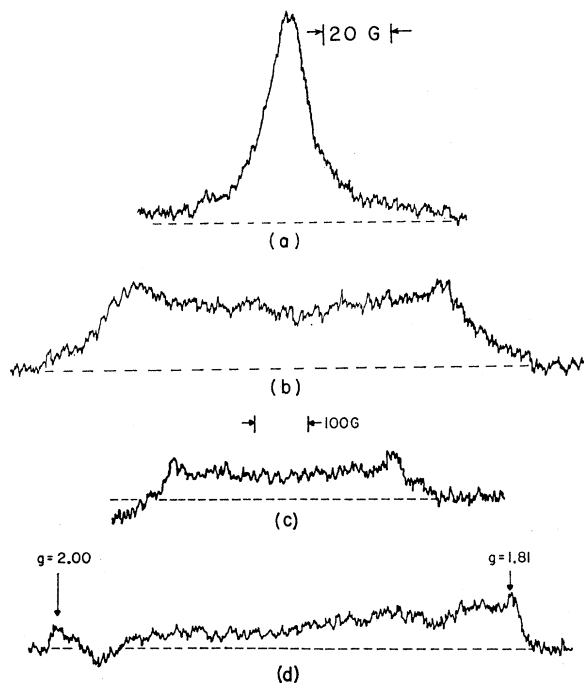


FIG. 4. Optically detected resonance signals observed in spectrum I of the 2E level of Cr^{3+} ; (a) $\mathbf{H} \parallel [111]$, (b) \mathbf{H} at 5° from $[111]$, (c) $\mathbf{H} \parallel [110]$, (d) $\mathbf{H} \parallel [001]$.

Spectrum II is dissimilar to I in the absence of the low-field portion of the resonance band, as is apparent from Fig. 5 in the traces taken at 25° from $[111]$. It will be shown below that spectrum II is approximately that which should be observed in optical detection for isolated Cr^{3+} ions, whereas spectrum I, which is observed in a majority of the samples investigated, results from the influence of cross-relaxation processes.

The resonance of the 2E level for the isoelectronic V^{2+} ion with $\mathbf{H} \parallel [111]$ is shown in Fig. 6, with experimental conditions similar to those holding for the data of Figs. 4 and 5. The resonance center is located at $g=1.860\pm 0.005$. The seven weaker lines in the spectrum are apparently the "forbidden" hyperfine transitions $\Delta m_l = \pm 1$. Their large intensity relative to the allowed transitions results from the nature of the de-

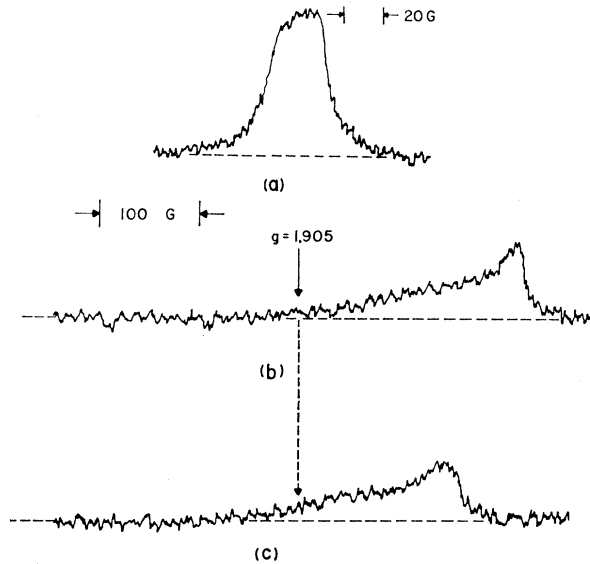


FIG. 5. Resonance signals observed in spectrum II of the 2E level of Cr^{3+} ; (a) $\mathbf{H} \parallel [111]$, (b) \mathbf{H} at 25° toward $[001]$, (c) \mathbf{H} at 25° toward $[110]$.

tection scheme, which measures the population change induced by the microwave transitions. In this case, the microwave power is at such a high level that this population change is nearly a maximum for the allowed transitions (that is, the saturated hole is approaching the inhomogeneous width of the lines), and the forbidden transitions are approaching this condition. A study of this spectrum as a function of microwave power gives an intensity ratio of the forbidden and allowed transitions of about 5×10^{-3} at low microwave powers, which is in good agreement with the ratio expected if the forbidden transitions are induced by the component of microwave magnetic field parallel to \mathbf{H} . These transitions are allowed by the mixing of electron and nuclear spin states by the hyperfine interaction itself. The separation of the eight allowed hyperfine components gives a hyperfine coupling constant for $\mathbf{H} \parallel [111]$ of $A = (90 \pm 1) \times 10^{-4} \text{ cm}^{-1}$.

No structure can be resolved in the V^{2+} resonance for \mathbf{H} more than a few degrees from $[111]$, although the position of the sharp low-field edge of the absorption band was followed for orientations of \mathbf{H} up to 25° from $[111]$ to confirm the expected anisotropy of

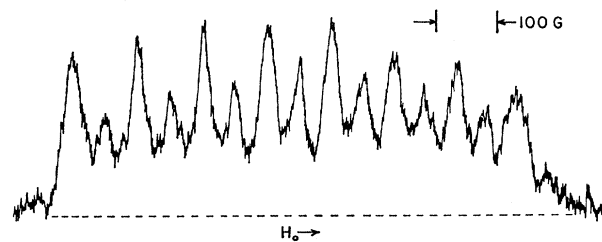


FIG. 6. ESR spectrum of the 2E level of V^{2+} with $\mathbf{H} \parallel [111]$.

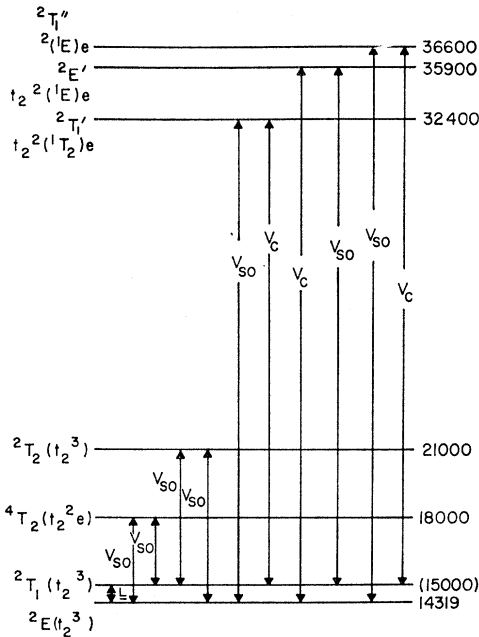


FIG. 7. Energies and strong crystal-field compositions of relevant states of $3d^3$. The ground 4A_2 level is not shown and is assumed to be at zero energy.

the g shift and hyperfine constant, which are discussed in Sec. IV.

IV. DISCUSSION

The explanation of these resonances and their anisotropy requires a consideration of the combined effects of the orbital moment admixed into 2E by interactions with higher-lying states of the d^3 configuration, the splitting of 2E by random lattice strains, selection rules for the circular-polarized fluorescence, and rate processes associated with microwave saturation and spin-lattice relaxation in 2E . These properties are considered in this section.

A. Magnetic Splitting

The crystal-field splitting of the $3d^3$ configuration is summarized in Fig. 7,⁸ which gives the positions and crystal-field notations for all of the states of importance to this discussion lying above the 4A_2 ground state, which is assumed to be at zero energy. The 2E level, like the ground 4A_2 state, has the t_2^3 crystal-field composition in the strong cubic-field limit. However, the free-ion Coulomb interaction couples the strong cubic-field states and admixes configurations such as t_2^2e into the 2E level. We adopt Clogston's⁹ notation and allow for this mixing with an interaction V_c which couples strong field states of the same symmetry and spin. The coupling of the levels of d^3 by V_c , V_{so} , the spin-orbit inter-

action, and \mathbf{L} , the orbital-momentum operator, are summarized in Fig. 7.⁹

It is apparent that, in the absence of V_c , the usual perturbation term leading to orbital-momentum admixture into 2E , $\langle {}^2E | \mathbf{L} | {}^2\Gamma \rangle \langle {}^2\Gamma | V_{so} | {}^2E \rangle$, vanishes, as there is no state ${}^2\Gamma$ coupled to 2E by both \mathbf{L} and V_{so} . There are, however, interactions involving V_c and V_{so} in higher order, which may give sizeable contributions. These are of the following three types:

$$\frac{\langle {}^2E | \mathbf{L} | {}^2T_1 \rangle \langle {}^2T_1 | V_c | {}^2T_1' \rangle \langle {}^2T_1' | V_{so} | {}^2E \rangle}{[W({}^2T_1) - W({}^2E)][W({}^2T_1') - W({}^2E)]}, \quad (1a)$$

$$\frac{\langle {}^2E | \mathbf{L} | {}^2T_1 \rangle \langle {}^2T_1 | V_{so} | {}^2T_2 \rangle \langle {}^2T_2 | V_{so} | {}^2E \rangle}{[W({}^2T_1) - W({}^2E)][W({}^2T_2) - W({}^2E)]}, \quad (1b)$$

$$\frac{\langle {}^2E | V_{so} | {}^4T_2 \rangle \langle {}^4T_2 | \mathbf{L} + 2\mathbf{S} | {}^4T_2 \rangle \langle {}^4T_2 | V_{so} | {}^2E \rangle}{[W({}^4T_2) - W({}^2E)]^2}, \quad (1c)$$

where $W({}^2T_1)$ is the energy of the 2T_1 level, etc. Terms like (1a) and (1b) lead to g shifts of identical symmetry, and those like (1c) give isotropic shifts. A simple estimate justifies the neglect of interactions similar to (1c), since their contribution is less than 1% of the total shift.

Since 2E is orbitally degenerate, the angular dependence of the Zeeman splitting must be deduced from a secular equation which may be obtained from the coupling coefficients of the cubic double group, either by direct calculation or from a spin Hamiltonian with $S' = \frac{3}{2}$. The basis functions for 2E are chosen to be $\langle E_u \pm \frac{1}{2} |$ and $\langle E_v \pm \frac{1}{2} |$, where E_u and E_v transform as $E_u \sim (3z^2 - r^2)$, $E_v \sim (x^2 - y^2)$. The primes denote the components along the applied magnetic field \mathbf{H} , which has direction cosines (l, m, n) relative to the cube axes.

If terms like (1c) are neglected, the Zeeman splitting is a function of only one empirical parameter α , and the approximate solution of the secular equation may be represented by a double-valued expression for g , which is identical to that given by Abragam and Pryce¹⁰ for Cu^{2+} :

$$g = 2 + 4\alpha [1 \pm (l^4 + m^4 + n^4 - l^2m^2 - l^2n^2 - m^2n^2)^{1/2}]. \quad (2)$$

In a spin-Hamiltonian formalism, the splitting, including the hyperfine interaction for V^{2+} , is described by the following Hamiltonian with an effective spin of $\frac{3}{2}$ ^{11,12}:

$$H = g_1\beta\mathbf{H} \cdot \mathbf{S} + g_2\beta \sum_{i=x,y,z} H_i S_i^3 + A_1 \mathbf{I} \cdot \mathbf{S} + A_2 \sum_{i=x,y,z} I_i S_i^3.$$

If the states of $S' = \frac{3}{2}$ are related to those of 2E by

¹⁰ A. Abragam and M. H. L. Pryce, Proc. Phys. Soc. (London) **A63**, 409 (1950).

¹¹ B. Bleaney, Proc. Phys. Soc. (London) **A73**, 939 (1959).

¹² F. S. Ham, G. W. Ludwig, G. D. Watkins, and H. H. Woodbury, Phys. Rev. Letters **5**, 468 (1960).

⁸ Y. Tanabe and S. Sugano, J. Phys. Soc. Japan **9**, 766 (1954).

⁹ A. M. Clogston, Phys. Rev. **118**, 1229 (1960).

$\frac{3}{2} \rightarrow (E_u, -\frac{1}{2}), \frac{1}{2} \rightarrow (E_v, \frac{1}{2}), -\frac{1}{2} \rightarrow -(E_v, -\frac{1}{2}),$ and $-\frac{3}{2} \rightarrow -(E_u, \frac{1}{2})$, then $g_1 = \frac{1}{3}(7+\alpha)$ and $g_2 = -\frac{4}{3}(1+\alpha)$.

The reduced matrix element α in Eq. (2) may be calculated by summing over all possible interactions of types (1a) and (1b). This has been done for Cr^{3+} , using the energy separations from Fig. 1 and the following parameters derived from optical data obtained¹³ in $\text{Al}_2\text{O}_3:\text{Cr}^{3+}$, which will be assumed to approximate those for $\text{MgO}:\text{Cr}^{3+}$:

$$\begin{aligned}\zeta &= (1/3i) \langle t_2 || 1 \cdot \mathbf{s} || t_2 \rangle = 140 \text{ cm}^{-1}, \\ \zeta' &= -(1/3\sqrt{2}i) \langle t_2 || 1 \cdot \mathbf{s} || e \rangle = 180 \text{ cm}^{-1}, \\ k &= 0.62, \quad B = 700 \text{ cm}^{-1},\end{aligned}$$

where ζ' and ζ are reduced matrix elements of the spin-orbit interaction, k is the orbital-reduction factor, and B is the Racah parameter characterizing the strength of the electronic Coulomb interaction. The result is $\alpha = -0.025$, which would lead to a g value for the $[111]$ resonance of Cr^{3+} of 1.90.

Sturge,⁴ in his study of the Zeeman effect of V^{2+} in MgO , has performed a similar calculation for V^{2+} by setting the trigonal-field parameter equal to zero in a program of Sugano and Peter¹⁴ which allows for configuration mixing among the 80 lowest levels of $3d^3$. The resulting g value for V^{2+} is 1.89. The agreement of these results with the experimental values of 1.905 for Cr^{3+} and 1.860 for V^{2+} is reasonable, considering that the parameters used in the calculation are derived primarily from fits to the positions and the magnetic- and trigonal-field splittings of the lowest levels of $3d^3$. Even then, there is some disagreement among the parameters needed to fit the trigonal-field splittings and those giving the correct Zeeman splittings of the 2E levels for Cr^{3+} and V^{2+} in Al_2O_3 .¹⁴ The Zeeman splitting in the cubic field, however, involves primarily coupling with the higher-lying states of t_2^2e for which the magnitudes of these parameters are only approximate.

For the applied field in a $\{110\}$ plane, Eq. (2) reduces to

$$g = 2 + 4\alpha [1 \pm (\cos^2\theta - \frac{1}{2} \sin^2\theta)], \quad (3)$$

where θ is the angle of \mathbf{H} to the $[001]$ axis along which E_u and E_v are assumed quantized. The form of the secular equation for this orientation of \mathbf{H} shows that the orbital eigenfunctions of the Zeeman interaction are E_u and E_v for all θ . This result is of importance in determining the resonance shapes for spectrum II of Sec. III.

B. Effects of Random Lattice Strain

To a first approximation, the 2E level of the d^3 ions is not affected by strain as a result of the symmetry properties of its strong-field t_2^3 configuration. However, the configuration mixing and spin-orbit coupling lead to a noticeable strain sensitivity, which has been meas-

ured and explained in detail by Schawlow *et al.*² for Cr^{3+} and by Sturge³ for V^{2+} . It is apparent from these studies that the lattice coupling is far too weak to lead to a strong Jahn-Teller effect,¹⁵ which is the dominating feature of other orbitally degenerate $3d$ ions such as Cu^{2+} .¹⁶ In this case, only random lattice strains have a noticeable effect on the resonance properties of the state.

A measure of the magnitude of these strain splittings is provided by the width of the R -line transition, which is about 0.5 cm^{-1} and is a result of almost equal contributions from the strain-induced shift of 2E relative to 4A_2 and a splitting of the degeneracy of 2E itself.² In resonance experiments performed at 24 GHz, this mean strain splitting of a few tenths of a wave number is considerably greater than the magnetic-field splitting of the orbital degeneracy which is given by Eq. (2), and is, at most, about 0.05 cm^{-1} for \mathbf{H} along $[001]$. However, the spin Zeeman interaction is about 0.8 cm^{-1} , which will tend to maintain the spin as a good quantum number. This effect is made more pronounced by the fact that strains of T_2 symmetry, which couple different spin states in conjunction with the spin-orbit coupling, are less effective than the E strains in splitting 2E by a factor of about 2.²

These approximations allow the assumption that the strain configuration at each site stabilizes a linear combination of the E_u and E_v orbitals. The approximate eigenfunctions of strain and magnetic field in this case are

$$\begin{aligned}(\cos\gamma | E_u \rangle + \sin\gamma | E_v \rangle) | \pm \frac{1}{2} \rangle, \\ (\sin\gamma | E_u \rangle + \cos\gamma | E_v \rangle) | \pm \frac{1}{2} \rangle,\end{aligned}$$

where the parameter γ may be related to the strain distribution at a given site. The splitting of these states by a magnetic field is given by the g values

$$\begin{aligned}g_1 &= \cos^2\gamma g(E_u) + \sin^2\gamma g(E_v), \\ g_2 &= \sin^2\gamma g(E_u) + \cos^2\gamma g(E_v).\end{aligned} \quad (4)$$

Equation (4) shows that the allowed magnetic transitions will have an energy splitting less than or equal to that given by Eq. (3), i.e., $[g(E_u) - g(E_v)]$. For all reasonable distributions of strain amplitudes, the distribution of γ in (4) results in a resonance shape with singularities at the positions of the magnetic doublet given by Eq. (3), which will lead to peaks in the resonance data at these positions. These effects are exactly what has been observed in the data. A plot of the measured separation of the peaks is shown in Fig. 8. The solid curve is calculated from Eq. (3), with $\alpha = -0.024$, which gives the correct g value for the resonance with $\mathbf{H} || [111]$. The reasonable fit confirms the expected form for the Zeeman splitting given by Eq. (2).

¹⁵ M. D. Sturge, in *Solid State Physics*, edited by F. Seitz and D. Turnbull (Academic Press Inc., New York, 1967), Vol. 20, p. 92.

¹⁶ M. C. M. O'Brien, Proc. Roy. Soc. (London) **A281**, 323 (1964).

¹³ S. Sugano and Y. Tanabe, J. Phys. Soc. Japan **13**, 880 (1958).

¹⁴ S. Sugano and M. Peter, Phys. Rev. **122**, 381 (1961).

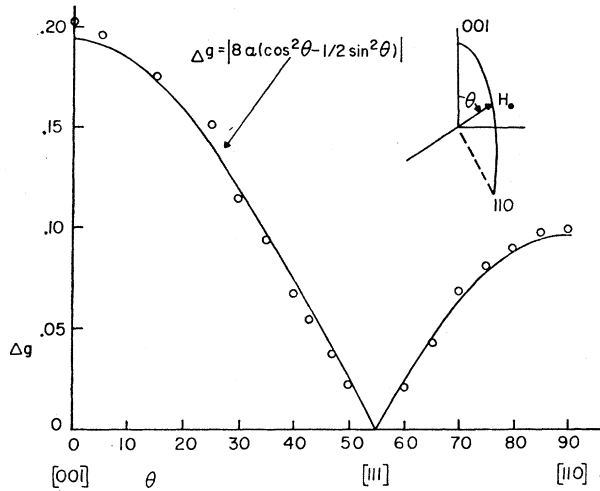


FIG. 8. Angular dependence of Zeeman splitting of the 2E level of Cr^{3+} for \mathbf{H} in a $\{110\}$ plane.

C. Anomalies in the Resonance Shape

Since E_u and E_v are the magnetic orbital eigenfunctions when the magnetic field is in the (110) plane, it follows that the resonance intensity near the extreme peaks of the resonance arises from those strain sites at which the strain eigenfunctions are nearly pure E_u and E_v , and the central portion arises from those sites where a linear combination of E_u and E_v are stabilized. Furthermore, as the resonance is detected as a change in circularly polarized light emitted by the excited ions, it is apparent that the details of the resonance shape will be influenced by the fluorescence selection rules and the nature of the population changes induced by the microwave transitions.

It can be shown from the selection rules for the magnetic dipole R -line transition that the net fractional

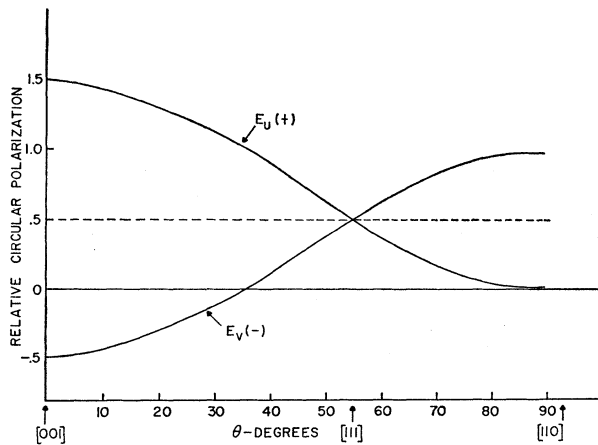


FIG. 9. Net relative circular polarizations along \mathbf{H} at an arbitrary temperature for the fluorescence from the E_u and E_v states with \mathbf{H} in a $\{110\}$ plane. θ is measured from $[001]$.

circular polarization at temperature T along the applied field, for \mathbf{H} in a $\{110\}$ plane, is

$$\left| \frac{I_{\text{RCP}} - I_{\text{LCP}}}{I_{\text{tot}}} \right| = \frac{1}{8} \left[\frac{1 - \exp(-2\beta H/kT)}{1 + \exp(-2\beta H/kT)} \right] \times \left[\frac{1}{2} \pm (\cos^2\theta - \frac{1}{2} \sin^2\theta) \right], \quad (5)$$

where the plus sign holds for the E_u orbital and the minus for E_v . This expression includes a sum over the intensities of all transitions between spin levels for each orbital state. The angular dependence of Eq. (5) is illustrated in Fig. 9.

The influence of the above results on the shape of the resonance will depend upon the nature of the population changes induced by microwave saturation. Figure 10 represents a typical set of nearly identical ion sites in which random strain has stabilized orbital states (a) and (b). At points far from the center of the broadened resonance, microwave saturation can occur in state (a), say, but not in (b), which will have a g value placing it on the other side of the resonance center.

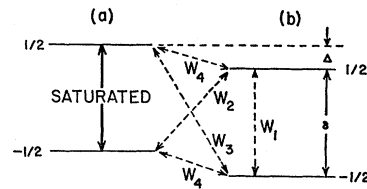


FIG. 10. Microwave saturation and thermal relaxation rates for 2E at a set of nearly identical strain sites.

The population changes induced by this saturation will depend on the relative magnitudes of the thermal relaxation rates W_1 , W_2 , W_3 , and W_4 . These rates can be estimated from the measured static-strain-splitting coefficients for the 2E level in MgO . The basis for such a calculation is that the transition from level γ_1 to γ_2 via the direct process is proportional to

$$| \langle {}^2E\gamma_2 | \mathbf{V}_1 : \tilde{\epsilon} | {}^2E\gamma_1 \rangle |^2,$$

where $\tilde{\epsilon}$ is the time-dependent strain tensor at the site, and \mathbf{V}_1 is the coefficient of the linear term in the strain expansion of the crystal-field energy for the 2E level. Writing ϵ in terms of the cubic strain bases, ${}^2e(\Gamma, \gamma) \mathbf{V} : \tilde{\epsilon}$ is expanded as

$$\tilde{\mathbf{V}} : \tilde{\epsilon} = \sum_{\Gamma, \gamma} V(\Gamma) C(\Gamma, \gamma) e(\Gamma, \gamma),$$

where the $C(\Gamma, \gamma)$ are normalized linear combinations of spherical harmonics transforming as $e(\Gamma, \gamma)$, whose matrix elements are the coupling coefficients $\langle \Gamma_3 \gamma_1 | \Gamma \gamma \Gamma_3 \gamma_2 \rangle$ as defined by Griffith.¹⁷ The matrix elements of this expression may be used to calculate

¹⁷ J. S. Griffith, *The Theory of Transition Metal Ions* (Cambridge University Press, Cambridge, England, 1961).

TABLE I. Strain-coupling matrix for 2E . The $e(\Gamma, \gamma)$ are normalized strain bases. $e(T_{2\pm 1}) = (\pm i/\sqrt{2})[e(T_{2x}) \pm ie(T_{2y})]$, $(T_{20} e) = ie(T_{2z})$, $T_{2z} = yz$, etc. E_u, E_v , and S_z quantized along $[001]$.

	$E_u, \frac{1}{2}$	$E_v, \frac{1}{2}$	$E_u, -\frac{1}{2}$	$E_v, -\frac{1}{2}$
$E_u, \frac{1}{2}$	$-V(E)e(E_u)$			
$E_v, \frac{1}{2}$	$V(E)e(E_v) + V(T_2)e(T_{20})$	$V(E)e(E_u)$		
$E_u, -\frac{1}{2}$	0	$\sqrt{2}V(T_2)e(T_{21})$	$-V(E)e(E_u)$	
$E_v, -\frac{1}{2}$	$-\sqrt{2}V(T_2)e(T_{21})$	0	$V(E)e(E_v) - V(T_2)e(T_{20})$	$V(E)e(E_v)$

the static, uniaxial strain splitting of 2E , and the $V(\Gamma)$ are obtained in this way from the measured stress splittings. The resulting strain matrix elements are summarized for reference in Table I. The $V(\Gamma)$ obtained from the stress data are: for Cr^{3+} , $V(E) = 660 \text{ cm}^{-1}$, $V(T_2) = 363 \text{ cm}^{-1}$; for V^{2+} , $V(E) = 1100 \text{ cm}^{-1}$, $V(T_2) = 174 \text{ cm}^{-1}$.

The strain bases $e(\Gamma, \gamma)$ may be expressed in terms of phonon operators, and the direct transition rates are calculated by the usual procedures.¹⁸ The results of such a calculation show that $W_2 \sim W_3 \sim 10W_4$ and $W_2 \sim 100W_1$. The first relation is the result of the small average magnitude of Δ compared with δ , giving a smaller density of phonon states at this energy. The second is dependent on the same assumptions leading to Eq. (4).

Using these estimates, it can be shown from simple rate equations that when the spin-level populations of orbital state (1a) are equalized by saturation, the spin levels of (1b) are cooled to the extent that the population difference of the two spin states is doubled from its thermal-equilibrium value at the temperatures used in the experiment. Since the circular polarizations of the fluorescence emitted from (1a) and (1b) will, in general, differ in sign, magnitude, or both, this effect results in a different sign or magnitude for the optical signal, depending upon whether saturation occurs in (1a) or (1b). A qualitative picture of the resonance shapes, taking account of these factors for $\mathbf{H} \parallel [001]$ and $\mathbf{H} \parallel [110]$, is shown in Fig. 11.

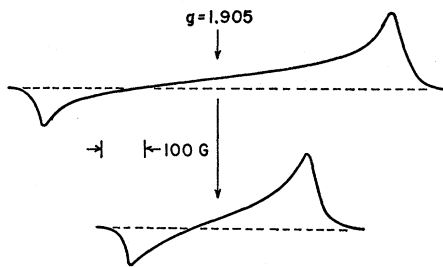


FIG. 11. Expected resonance shapes for optical detection with thermal relaxation at 1.5°K . Upper curve, $\mathbf{H} \parallel [001]$; lower curve, $\mathbf{H} \parallel [110]$.

¹⁸ J. H. Van Vleck, Phys. Rev. **57**, 426 (1940).

The presence of the “negative” signal due to detection of the ground-state resonance by means of reabsorption of R -line fluorescence prevents an unambiguous verification of the negative signal expected from 2E in any of the samples studied. However, the data of Fig. 5 for spectrum II at 25° to $[111]$ show asymmetries which are qualitatively characteristic of those expected from the above considerations, in that the low-field portion of the resonance is considerably reduced in intensity.

The origin of the completely symmetric resonance of Fig. 4 is apparently connected with the coupling of the 2E level to the large amounts of Fe^{2+} in this sample. Evidence for this assertion is provided by the large Fe^{2+} resonance observed in this sample and also by the detection of a large change in circular polarization of the R -line fluorescence caused by microwave absorption in the broad Fe^{2+} resonance at $g = 3.4$.¹⁹ Both of these effects are very much weaker in the sample from which the data of Fig. 5 were obtained. The symmetry of the signals observed in Fig. 4 can be attributed to this coupling to Fe^{2+} if a very rapid cross-relaxation process is assumed to be in parallel with W_4 and involves spin transitions in two Fe^{2+} ions, with strain splittings differing in magnitude by the amount Δ in Fig. 10. The fact that the strain width of the Fe^{2+} ground state is roughly comparable with that of 2E makes this a plausible mechanism.

Further evidence that the data of Fig. 5 are representative of a thermally relaxing 2E level is that the measured spin-lattice relaxation rate for this sample is linear in T up to at least 4.2°K , and T_1 has a magnitude at 1.5°K of $600 \mu\text{sec}$, which compares well with the value of $550 \mu\text{sec}$ estimated from the static-strain coupling coefficients. The measured T_1 of sample I, however, was less than $50 \mu\text{sec}$ at 1.5°K .

D. Hyperfine Structure of V^{2+}

The 99.75%-abundant V^{51} nucleus has been found to have a hyperfine coupling constant of $74.24 \times 10^{-4} \text{ cm}^{-1}$ for the orbital singlet ground state in MgO .²⁰ The hyperfine constant for 2E will differ from this by an orbital

¹⁹ W. Low, Ann. N.Y. Acad. Sci. **72**, 69 (1958).

²⁰ W. Low, Phys. Rev. **101**, 1827 (1956).

contribution A_L , which is related to the g shift in 2E by²¹

$$A_L = 2\gamma\mu_N\mu_B\Delta g\langle r^{-3} \rangle, \quad (6)$$

where γ and μ_N are the nuclear gyromagnetic ratio and nuclear magneton, respectively, μ_B is the Bohr magneton, $\Delta g = g - 2.0023$, and $\langle r^{-3} \rangle$ is an average over the $3d$ wave function. Freeman and Watson²² have calculated $\langle r^{-3} \rangle = 2.75$ a.u. from the free-ion Hartree-Fock wave functions. This value and the measured g shift

²¹ A. Abragam and M. H. L. Pryce, Proc. Roy. Soc. (London) **A205**, 135 (1951).

²² A. Freeman and R. E. Watson, in *Magnetism*, edited by G. Rado and H. Suhl (Academic Press Inc., New York, 1965), Vol. IIA.

with \mathbf{H} along $[111]$ used in Eq. (6) give a predicted orbital contribution $A_L = -17 \times 10^{-4} \text{ cm}^{-1}$, which is to be added to the core-polarization hyperfine interaction, which is also negative. The total calculated hyperfine constant thus obtained is $A = 91 \times 10^{-4} \text{ cm}^{-1}$. This is in excellent agreement with the measured value of $90 \times 10^{-4} \text{ cm}^{-1}$, and implies that the calculated $\langle r^{-3} \rangle$ is accurate to at least 5% for this system.

ACKNOWLEDGMENTS

The author is indebted to Professor R. H. Silsbee and Dr. D. L. Cowan for many helpful discussions and suggestions concerning this work.

Three-Spin Cross Relaxation in $\text{Cr}^{3+}:\text{K}_3\text{Co}(\text{CN})_6$ †

JAN M. MINKOWSKI

Department of Electrical Engineering, The Johns Hopkins University, Baltimore, Maryland

(Received 2 November 1967)

An experiment designed to study the three-spin cross relaxation (CR) rate without interference from much faster two-spin CR processes is described. The study was performed on the electron spin system Cr^{3+} in $\text{K}_3\text{Co}(\text{CN})_6$ and the CR rate was determined for a range of concentrations 0.036–1.030% and an energy imbalance range of ± 680 MHz from the harmonic point. Comparison with Bloembergen's "hybrid" method (in the present application by an exact computation of the second moments of the shape functions) shows good agreement for concentrations in the range 0.036–0.384%. For higher concentrations, this theory does not explain the data. The experimental results are also in disagreement with a theory of Grant's, which gave a good account of several previous two-spin CR experiments.

I. INTRODUCTION

TWO theories of cross relaxation (CR) in spin systems have been advanced. In both theories the dipolar and exchange interactions play dual roles; their secular parts broaden the energy levels of the system of uncoupled spins and the nonsecular parts cause transitions ("flip-flops") of spins. In 1958, Bloembergen *et al.*¹ introduced a theory of CR (the so-called "hybrid method") which was an extension of previous theories of paramagnetic line broadening. The CR rate in this theory is given as $W(\omega) = (2\pi/\hbar) |\langle i | H_{\text{dip}}^{\text{NS}} | f \rangle|^2 g(\omega)$, in which the nonsecular part $H_{\text{dip}}^{\text{NS}}$ is the interaction operator and $g(\omega)$ is the shape function, which Bloembergen *et al.*¹ compute (for a two-spin process) by the folding of two paramagnetic line shapes involved in the CR process. Instead of a convolution, Kiel,² Kopvillem,³ and Hirono⁴

have utilized the method of moments^{5,6} of the theory of paramagnetic line broadening. In diluted spin systems, of concentration f , the moments of the shape function are polynomials in f with leading terms which are concentration-independent.⁷ The shape of $g(\omega)$ in diluted systems has thus been assumed to be concentration-independent. The magnitude of the CR rate is proportional to f^{n-1} , where n is the order of the interaction (i.e., the number of spins involved in a single process); $n-1$ is also known to be the order of perturbation theory necessary to determine the matrix element of the transition operator. The hybrid method does not require exact conservation of Zeeman energy in a single process. CR transitions can occur away from the harmonic coincidence of the Zeeman transitions; the balance of energy is achieved by a dynamic rearrangement of the entire lattice. In practice, for systems in which S_z is not a good quantum number, only the first and second moments of $g(\omega)$ can be computed. The ratio of the two is then used as the criterion of whether

* This research was supported by the Electromagnetic Warfare Branch, Air Force Avionics Laboratory, Air Force System Command, U.S. Air Force, under Contract No. AF33(657)11029.

¹ N. Bloembergen, S. Shapiro, P. S. Pershan, and J. O. Artman, Phys. Rev. **114**, 445 (1958).

² A. Kiel, Phys. Rev. **120**, 137 (1960).

³ U. K. Kopvillem, Fiz. Tverd. Tela **2**, 1829 (1960) [English transl.: Soviet Phys.—Solid State **2**, 1653 (1960)].

⁴ M. Hirono, J. Phys. Soc. Japan **16**, 766 (1961).

⁵ J. H. Van Vleck, Phys. Rev. **74**, 1168 (1948).

⁶ M. H. Pryce and K. W. Stevens, Proc. Phys. Soc. (London) **A63**, 36 (1950).

⁷ A general application of the method of moments to the CR problems can be found in J. M. Minkowski, dissertation, Physics Dept., The Johns Hopkins University, 1963 (unpublished).